New Journal of Physics

The open access journal at the forefront of physics

PAPER

Biofilm formation in geometries with different surface curvature and oxygen availability

Ya-Wen Chang[1], Alexandros A Fragkopoulos[1], Samantha M Marquez[2], Harold D Kim[1], Thomas E Angelini[3] and Alberto Fernández-Nieves[1]

[1] School of Physics, Georgia Institute of Technology, Atlanta, GA, USA
[2] Branford College, Yale University, New Haven, CT, USA
[3] Mechanical and Aerospace Engineering, University of Florida, Gainesville, FL, USA

E-mail: alberto.fernandez@physics.gatech.edu and ya-wen@physics.gatech.edu

Abstract

Bacteria in the natural environment exist as interface-associated colonies known as biofilms . Complex mechanisms are often involved in biofilm formation and development. Despite the understanding of the molecular mechanisms involved in biofilm formation, it remains unclear how physical effects in standing cultures influence biofilm development. The topology of the solid interface has been suggested as one of the physical cues influencing bacteria-surface interactions and biofilm development. Using the model organism *Bacillus subtilis*, we study the transformation of swimming bacteria in liquid culture into robust biofilms in a range of confinement geometries (planar, spherical and toroidal) and interfaces (air/water, silicone/water, and silicone elastomer/ water). We find that *B. subtilis* form submerged biofilms at both solid and liquid interfaces in addition to air-water pellicles. When confined, bacteria grow on curved surfaces of both positive and negative Gaussian curvature. However, the confinement geometry does affect the resulting biofilm roughness and relative coverage. We also find that the biofilm location is governed by oxygen availability as well as by gravitational effects; these compete with each other in some situations. Overall, our results demonstrate that confinement geometry is an effective way to control oxygen availability and subsequently biofilm growth.

1. Introduction

Bacterial biofilms are interface-associated, bacteria conglomerates enclosed in self-produced extra-cellular polymeric substance (EPS) that are ubiquitous in natural and industrial environments [1, 2]. Biofilms play an important role in global ecology [3], for instance as nutrients in soils, sediments, oceans and fresh water. However, they are also notorious for causing industrial pipe fouling [4], tooth decay [5], plant infections [6], and hospital-acquired infections [7]. Infectious disease caused by biofilm indwelling in medical devices is especially problematic due to their high antibiotic resistance [8]. Understanding how the physical conditions of the environment modulate biofilm growth is essential to designing preventive measures for clinical and industrial contamination.

Physical factors such as substrate topography and hydrodynamics have been shown to govern biofilm formation. Micro- and nano-scale substrate topology regulates the initial attachment and adhesion of bacteria to solid surfaces [9, 10], which is the first step in surface colonization. Beyond the adhesion stage, mechanical shear due to flow could enhance or diminish biofilm formation [11–14]. It has been shown that both *S. aureus* and *P. aeruginosa* form biofilm streamers inside microfluidic devices with curved channels, bridging gaps between corners, which in turn prevent flow [13, 15]. On the other hand, much less is known about the physical regulation of biofilm formation in completely stagnant conditions.

Biofilms, although commonly refereed to as solid-attached structures could, in principle, be associated with any type of interface including air–liquid, liquid–liquid, solid–liquid, or air–solid interfaces. Natural isolates of *B. subtilis* have been well characterized for their ability to form robust air–liquid interface biofilms, also known as

pellicles [16, 17]. *B. subtilis* biofilms also grow on solid–air interfaces of agar containing water and nutrients, where single biofilm patches expand radially as they grow in response to nutrient gradients. Solid–air biofilms display heterogeneous distributions of cell phenotype within the biofilm and variation in EPS production, which match the spatial gradients of nutrient levels [18–20]. Unlike *P. aeruginosa*, there are few reports on submerged *B. subtilis* biofilms possibly due to their inability to form solid substrate-associated biofilms under flow conditions [17].

Here we investigate *B. subtilis* biofilm formation on different interfaces within various confinement geometries. Shaping of the confinement geometry relies on the novel use of yield-stress materials (YSM), where curved interfaces can be readily fabricated. We examined biofilm growth on several types of interfaces with both similar and dissimilar geometries. Comparing the array of biofilm parameters for the different systems, with corresponding sets of oxygen accessibility and the presence of gravity, we find that it is both these effects that mostly control where the biofilm grows. This indicates that it is possible to utilize large scale geometric features to regulate biofilm growth. Additionally, we find that the biofilm roughness and its relative surface coverage are higher on curved interfaces.

The rest of the paper is organized as follows. The materials and methods section describes the general experimental procedure of cell culture, substrate fabrication and data processing using our own programs. The results section focuses on the biofilm data, whilst the discussion section includes the detailed analysis and physical interpretation of our observations. We end the paper with conclusions and some final remarks.

2. Materials and methods

2.1. Bacteria strain and culture conditions
We use a dual fluorescent reporter strain of *B. subtilis* NCIB3610 in this study. The reporter construct includes a yellow fluorescent protein (YFP)-fused component (*tapA*) of the extracellular matrix and a cyan fluorescent protein (CFP)-fused component (*hag*) of flagella. The same strain has been used previously to monitor changes in EPS production (via YFP) and the change in cell motility (via CFP) in *B. subtilis* biofilms [19–21]. YFP reporter enables visualization of biofilm morphologies. Bacteria cells were streaked from a −80 °C frozen stock onto a Luria Bertani (LB) plate solidified with 1.5% agar. After incubation at 37 °C for 13 h, a single colony was inoculated in LB liquid medium. The cells were grown in LB at 37 °C to exponential phase with shaking for 3 h, until the transmission at 600 nm of the bacteria suspension decreased to ∼0.1.

2.2. Growing biofilm in different geometries
Cells in the LB shaking culture were diluted ten-fold with minimal salts glycerol glutamate (MSgg) liquid medium. The inoculated MSgg medium was then transferred to a glass-bottomed microwell plate or injected into silicone-based YSM consisting of a silicone-elastomer blend (9041, Dow Corning) and 10 cSt silicone oil. Samples were incubated statically at 35 °C for 2 days to enable biofilm development. Rectangular microwells provided flat substrates for cells to attach to and proliferate. The substrates could be solid, liquid, or air, depending on the boundary conditions imposed in the experiment (figure 1(a)). For example, layering the cell solution with silicone oil changes the upper liquid–air interface to a liquid–liquid interface. Curved substrates were fabricated through shearing YSM with a metallic needle while simultaneously injecting the cell solution. We note that a YSM behaves like a liquid when the applied stress is higher than its yield stress, which with our materials is in the range 10 to 100 Pa, and exhibits solid-like behavior when the external stress has been removed. To grow cells inside spherical droplets, we simply inject the desired volume of cell solution inside a YSM and subsequently remove the injection needle. To grow cells in toroidal-shaped droplets, the inoculated MSgg medium was injected into a rotating bath of YSM. This resulted in the formation of a curved jet that eventually closed onto itself to form a toroidal droplet containing living cells (figure 1(b)) [22]. The stability of the droplet against surface tension instabilities is provided by the elasticity of the surrounding medium [23]. We note, however, that the droplets are usually never a perfect torus. Instead, they are toroidal. As a result, they rarely have a circular cross-section, but rather are slightly elongated due to the shear that is involved in the generation process and the presence of the YSM, which stabilizes surface distortions with large radii of curvature. The surfaces are, however, locally smooth due to the interfacial tension between the cell solution and the YSM.

2.3. Biofilm studies and morphology analysis
The container cells were examined using an inverted optical microscope (Zeiss Axio-observer A1) equipped with a CCD camera. Fully developed biofilms expressing high levels of *tapA*-YFP were imaged using a confocal laser scanning microscope (CLSM, Zeiss LSM 510 system) with lateral and axial resolutions of 1.76 and 3.43 μm, respectively. Image data was captured using Zen software (Zeiss) and processed with custom written MATLAB codes. 3D rendered images were reconstructed from *Z*-stacks using Zen light (Zeiss). Biofilm morphology was
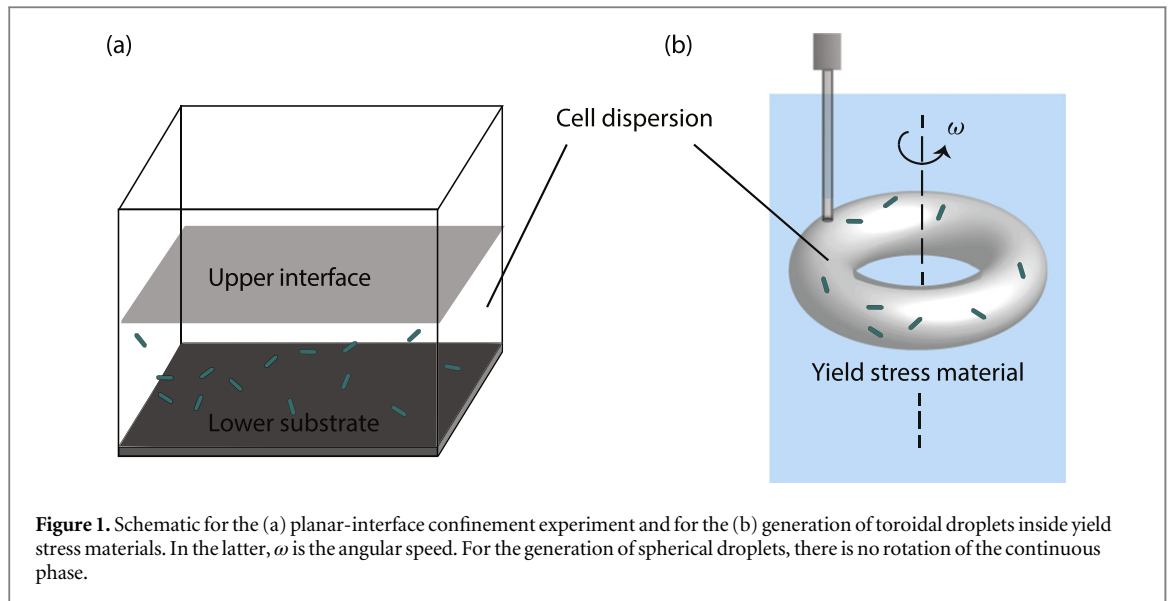
Figure 1. Schematic for the (a) planar-interface confinement experiment and for the (b) generation of toroidal droplets inside yield stress materials. In the latter, ω is the angular speed. For the generation of spherical droplets, there is no rotation of the continuous phase.

quantified with several parameters [24], including: (i) mean thickness, which identifies the maximum distance from the substrate in the direction normal to the substrate where there is biofilm, thus excluding all pores and voids within the biofilm; (ii) roughness, a quantity calculated from the thickness distribution and that describes the heterogeneity of the biofilm; (iii) substratum coverage, the percentage of substrate area occupied by the biofilm; (iv) surface-to-volume ratio, which reflects the fraction of biofilm area that is exposed to the nutrients; and (v) bio-volume or overall volume of the biofilm, which provides an estimation of the total biomass in the biofilm.

2.4. Confocal data analysis

The first step in confocal image processing is setting an intensity threshold and a cutoff value of the cosize or connected volume size. Thresholding yields a matrix with components that are one, for positions with biomass where the original intensity is equal to or above the set threshold, and components that are zero otherwise. Cosize identifies the minimum number of connected voxels with biomass that we attribute as being part of the biofilm. Applying a cosize cutoff can be seen as a filtering process that removes biomass voxels which are not considered as part of the biofilm. The bio-volume is calculated from the total number of biomass voxels in the biofilm multiplied by the voxel size. We define substratum coverage, Θ, as the fraction of area covered by biomass. We note that substrate here is generally defined as the interface that supports biofilm growth. For curved interfaces like the sphere and the toroid, the biofilm can only form on the lower half surface due to gravity, and hence we do not consider the uncovered part as part of the substrate. The substratum coverage is calculated as $\Theta = A_{b,s}/A_t$, where $A_{b,s}$ is the biofilm area at the substrate and A_t is the total substrate area. Point thickness, L_i, is measured by locating the highest biomass voxel along the normal of the substrate. Mean thickness L is calculated by number averaging individual thickness measurements. The biofilm roughness is defined as $R = \frac{1}{N}\sum_{i=1}^{N}\frac{|L_i - L|}{L}$, where N is the number of thickness measurements. Biofilm surface-to-volume ratio is defined as the exposed biofilm area, $A_{b,e}$, divided by the bio-volume, V_b. Note that $A_{b,e}$ is the biofilm area exposed to the nutrients, which includes all borders of the biofilm except for the border on the substrate. The sum of $A_{b,e}$ and $A_{b,s}$ gives the total surface area of the biofilm, A_b.

For biofilms on spherical surfaces, these quantities are obtained differently due to the interface being curved rather than being a simple horizontal plane. Thresholding and cosize selection is performed for the entire image stack, resulting in a three-dimensional matrix that represents the biofilm structure, as shown in the comparison between the rendered confocal image and the re-constructed image in figures 2(a)–(c). The bio-volume is calculated in the same fashion as described in the previous paragraph. To calculate other biofilm parameters, the data is treated as follows. We first locate the lowest point of the substrate with biomass and subsequently acquire the bottom layer of the biofilm (see figure 2(d)). We then generate a surface by interpolation that is reminiscent of the liquid–substrate interface (see figure 2(e)). Finally, we perform a smoothing of this surface to better capture the actual interface [25] (figure 2(f)). Once the spherical interface is defined, we can calculate the total substrate area A_t from the smaller area elements defined by the surface vectors $\vec{u}_1, \vec{u}_2, \vec{w}_1$ and $\vec{w}_2$ (figure 2(g)), $\Delta A = \frac{1}{4}(|\vec{u}_1 \times \vec{w}_1| + |\vec{u}_2 \times \vec{w}_2| + |\vec{u}_1 \times \vec{w}_1| + |\vec{u}_2 \times \vec{w}_2|)$, and summing over the area fraction where biofilm forms. We can also calculate the biofilm thickness, measured along the normal to the surface, at each point (see

Figure 2. (a)–(f) Procedure for confocal data processing of the biofilm on a curved surface using an inverted spherical cap as an example. The color scale of the reconstructed images indicates the z-position, in microns, of the substrate covered by biofilm. (g) Illustration of a curved 3D surface with surface area element given by vectors $\vec{u}_1, \vec{u}_2, \vec{w}_1$ and $\vec{w}_2$.

Figure 3. (a) Schematic of a torus with the *xyz* reference frame together with a toroidal surface reconstruction projected onto the *xy*-plane. The inner and outer parts of the torus are defined from the center line indicated on the graph, which is the locus of lowest points in the toroidal substrate. The color scale indicates the *z* position, in microns, of the substrate covered by biofilm. (b) Schematic illustrating the relevant geometric quantities used for describing the properties of the biofilm on the sphere.
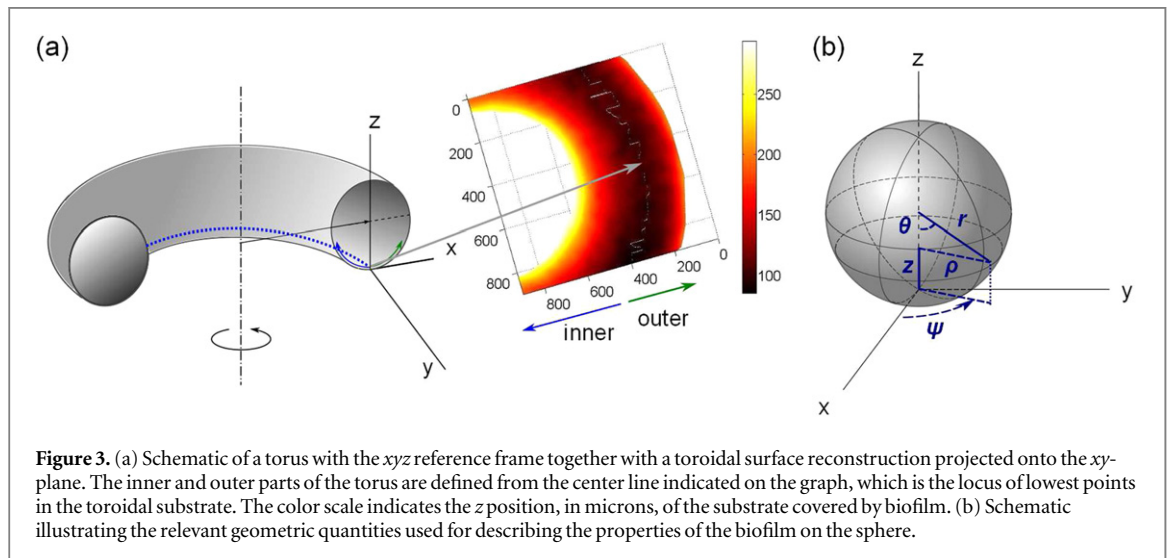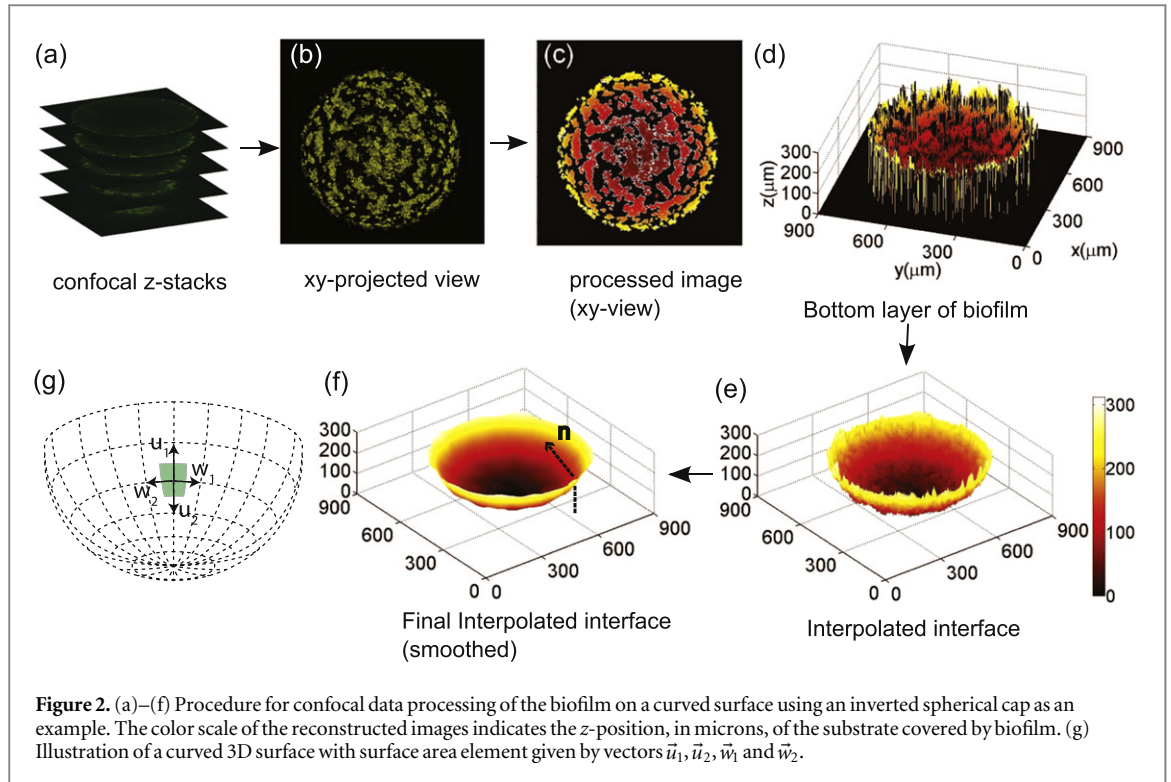
figure 2(f)). The mean biofilm thickness results from weighting the biofilm thickness over the biofilm area: $L = \frac{1}{A_{b,s}} \frac{1}{N} \sum_{i=1}^{N} L_i \Delta A$. The biofilm roughness is calculated using the same averaging process. In addition to performing this global averaging, we are also interested in the thickness and roughness profiles with height z, measured from the bottom of the spherical substrate. Based on the azimuthal symmetry of the system, we obtain these by averaging along the azimuthal direction.

In the case of the toroidal geometry, data processing and analysis is conducted as for the spherical case. However, thickness and roughness profiles are divided into an inner and an outer region, as indicated in figure 3(a). The division line is defined as the line made with the lowest points of the toroidal interface. This distinction is required for the case of toroids, since these lack constancy of curvature. Inner and outer then refers to regions of negative and positive Gaussian curvature, respectively. We also average the thickness and roughness profiles azimuthally, to obtain the profiles as a function of the height z, which is also measured from the lower point of the toroidal substrate (figure 3(a)).
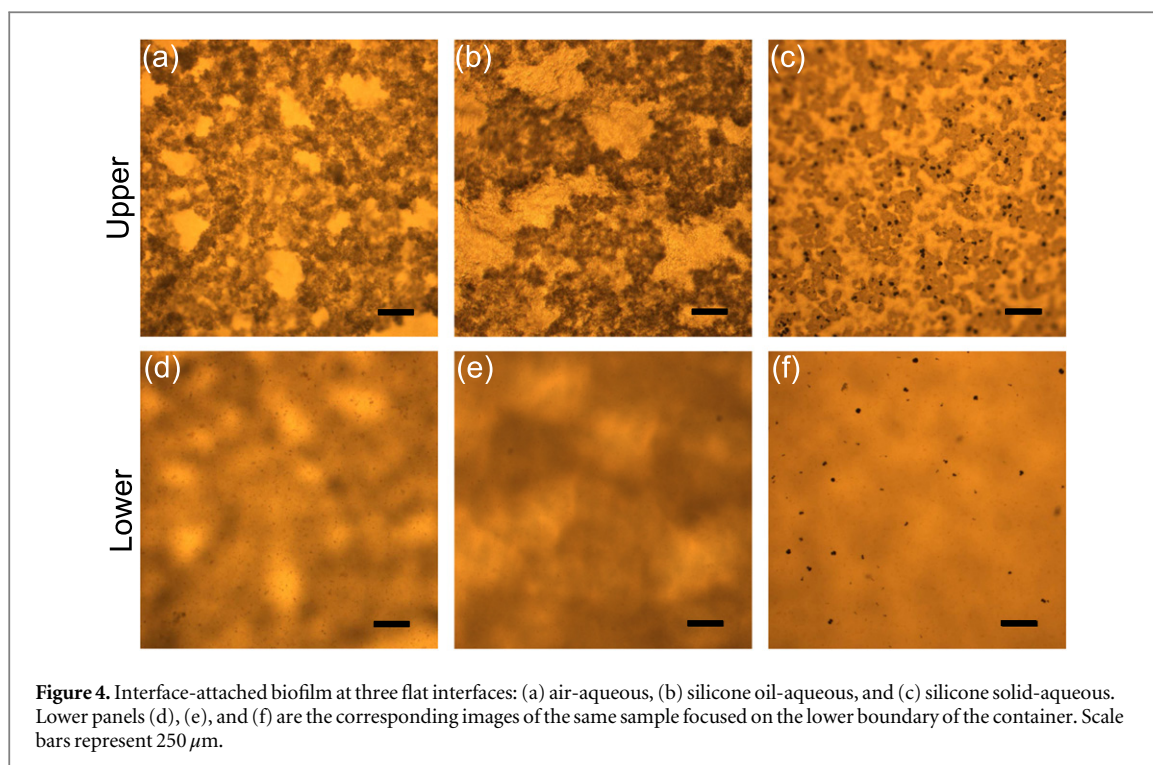
Figure 4. Interface-attached biofilm at three flat interfaces: (a) air–aqueous, (b) silicone oil–aqueous, and (c) silicone solid–aqueous. Lower panels (d), (e), and (f) are the corresponding images of the same sample focused on the lower boundary of the container. Scale bars represent 250 μm.

3. Results

3.1. Biofilm formation on flat interfaces

In standing culture, after a couple hours of incubation, a small population of bacteria cells bound to the bottom substrate of the microwell, while many more attached to the air interface, forming several thin, web-like colonies. The floating microcolonies developed over the course of 2 days into robust pellicles, while no significant biofilm growth was observed at the bottom substrate, as shown in figures 4(a), (d). The darker regions in figure 4(d) are the shadows of the biofilm located at the upper air–water interface. Modifying the hydrophobicity of the bottom substrate by coating it with silicone YSM yielded a similar outcome: the formation of a pellicle rather than a submerged biofilm. To examine the ability of *B. subtilis* to form biofilms in submerged systems, inoculated cell solution in microwells was topped with silicone oil and silicone YSM to create liquid–liquid and liquid–solid interfaces, respectively. Both microwells showed biofilm formation exclusively at the upper interface, as shown in figures 4(b), (e) and 4(c), (f). Note that the shadow from the biofilm is less significant in figure 4(f) than in figures 4(d) or (e), indicating a thinner biofilm at the upper silicone solid interface. Biofilm growth at the liquid–liquid interface is qualitatively comparable to that at the air–liquid interface, whereas the solid–liquid interface biofilm appears to mature earlier, as indicated by the formation of spores (black spots in figures 4(c), (f)).

The 3D structure of the biofilms, as visualized with EPS producing bacteria in figure 5, indicates that the structural heterogeneity of the biofilms depends on the interface the colony attaches to. Floating biofilm covers almost the entire air–liquid interface and displays several protruding structures as large as several hundred microns (figure 5(a)). On the contrary, the solid-attached biofilm appears to consist of connected cell clusters of varying size (figure 5(b)), and a reduced thickness and bio-volume compared to those of the pellicles, as shown in the first and fourth columns in table 1. We attribute this to the less favorable oxygen conditions in the latter environment; this is consistent with the observed transformation of active cells into spores.

Under usual biofilm forming conditions *B. subtilis* reduces surface tension via biosurfactant production. Surface tension reduction is a potential driving force for bacteria spreading and biofilm formation on air–water interfaces. From our results, it appears that surface tension does not play a determinant role here as we observe biofilm growth at air–water, silicone oil–water, as well as silicone solid–water interfaces. Another potential driving force would be oxygen. Aerobic respiration of bacteria results in rapid oxygen depletion in non-aerated standing cultures and a subsequent modification of the oxygen profile in the liquid medium [26]. We indeed find biofilm in more oxygenated regions; these correspond to the air–liquid, silicone oil–liquid and silicone solid–liquid interfaces of our microwells. In addition, the reduced biofilm growth, reflected in a decrease of L and V_b as the interface changes from the air–liquid to the silicone oil–liquid and the silicone solid–liquid also reflects the increasingly limited oxygen diffusion through these interfaces. Consistent with these results, it has
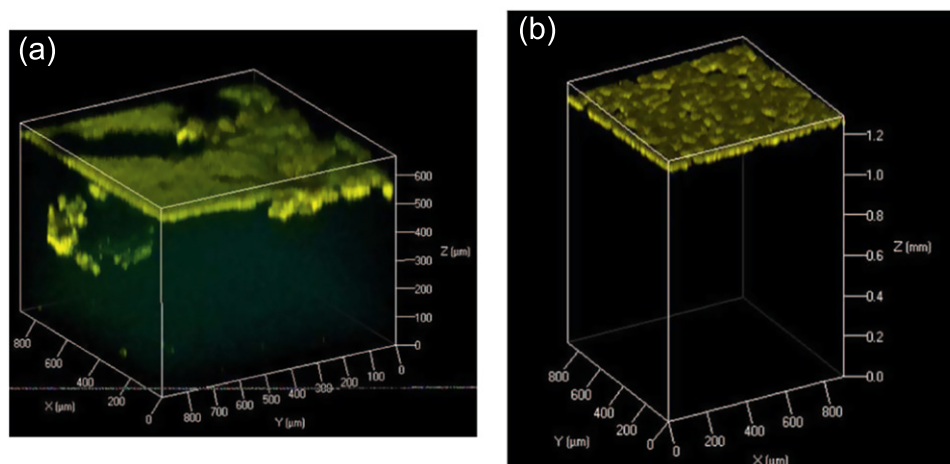
Figure 5. Three-dimensional biofilm structures obtained with *B. subtilis* on (a) air-aqueous and (b) silicone solid-aqueous interfaces. The acceleration of gravity is $\vec{g} = -g\hat{z}$.

Table 1. Summary of biofilm variables: average thickness L and maximum thickness $L_{\max}$, biofilm roughness R, bio-volume V_b, substratum coverage Θ, relative coverage Θ_{rel}, surface-to-volume ratio $A_{b,e}/V_b$, and bio-volume over total biofilm surface area V_b/A_b.

Confinement	L (μm)	$L_{\max}$ (μm)	R	V_b [a] (μm^3)	Θ (%)	Θ_{rel} (μm^2)	$A_{b,e}/V_b$ (μm^{-1})	V_b/A_b (μm)
Planar-air	89.3	474.9	0.41	0.0184	99.8	0.25	0.22	75.4
Planar-liquid	58.1	148.4	0.38	0.0130	93.7	0.23	0.09	56.6
Planar-solid	40.4	74.2	0.24	0.0082	79.3	0.19	0.09	42.1
Spherical-solid	23.1	82.7	0.48	0.0238	66.8	1.62	0.17	16.9
Toroidal-solid	21.6	78.3	0.51	0.0231	68.2	1.35	0.17	17.0

[a] This is the biovolume per 1 μm^3 of inoculate volume.

been shown that oxygen levels in microchambers can have an impact on the capability of bacteria to form stable and evenly distributed *P. aeruginosa* biofilms [27].
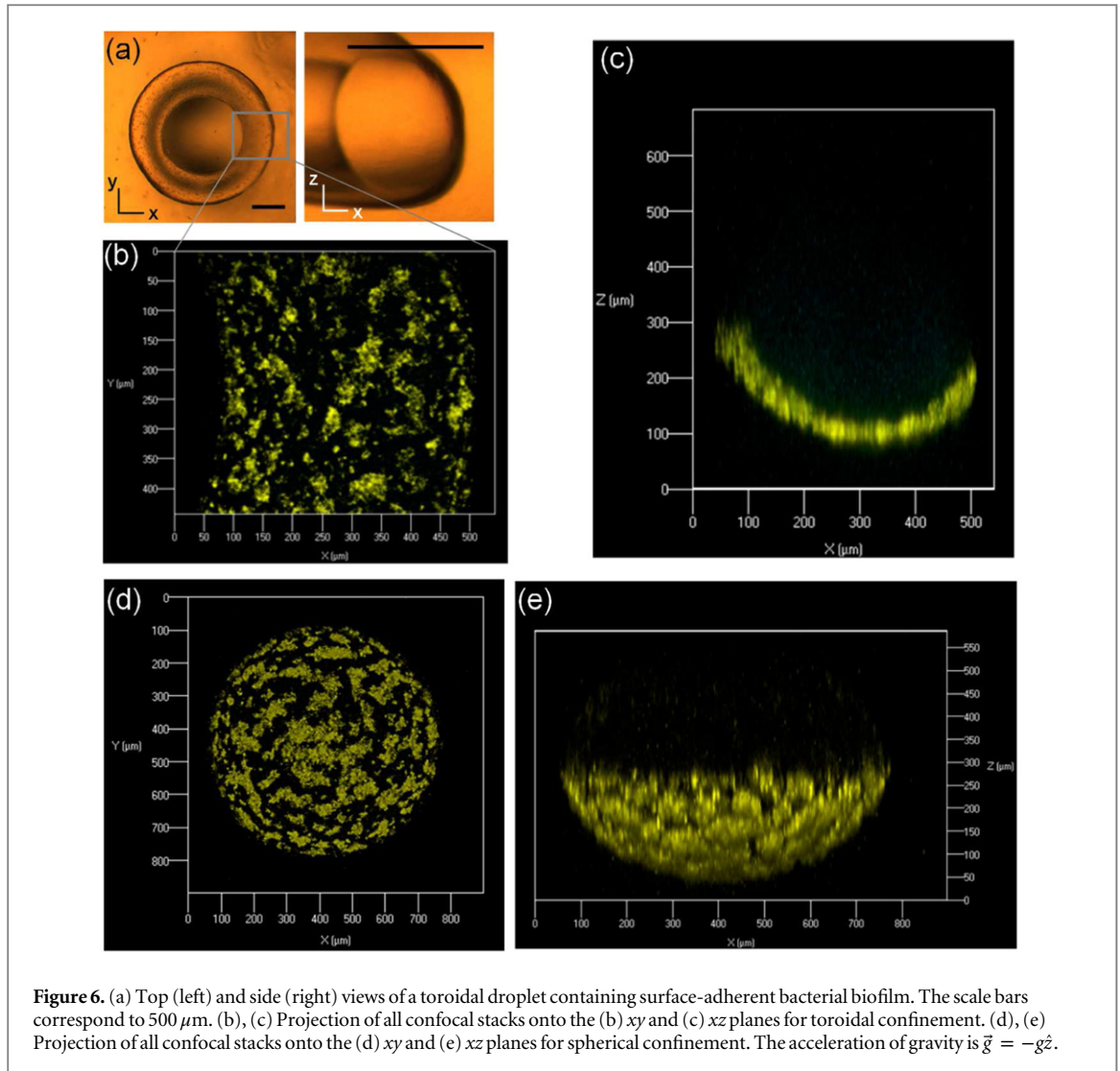
3.2. Formation of submerged biofilms in spherical and toroidal geometries

We also determine biofilm growth in non-planar geometries. In these experiments, the cell solution is encapsulated by silicone YSM in either spherical or toroidal confinement geometries. In these confinements, bacteria attach to the silicone interface and increase EPS production, as evident from the strong YFP fluorescence, which is comparable to that seen in planar biofilms. Figure 6 demonstrates the formation of surface-associated biofilms in these curved interfaces. Figure 6(a) shows bright field images of a biofilm-containing toroid, viewed from the top (left image) and viewed from the side (right image). Note that the cross-section of the torus is not perfectly circular. Confocal images were acquired for sections of the torus at different heights . The projection of all these confocal stacks show that the biofilm formed is patchy (figure 6(b)). The vertical cut of the stack further illustrates that the biofilm only grows on the lower part of the torus and that it grows to a higher height in its inner compared to its outer region (figure 6(c)). The observed asymmetry in biofilm growth correlates well with toroid cross-section, which is steeper in its outside than in its inside (figure 6(a), right image). Biofilms in spherical droplets also have a patchy texture and also only cover the lower part of the available surface (figures 6(d), (e)).

4. Discussion

4.1. Biofilm properties and positional roughness in various geometries

To quantify biofilm morphology in different geometries, we identify cell clusters associated with the biofilm (YFP) and reconstruct biofilm images from the CLSM optical sections. For biofilms on flat interfaces, thickness is measured directly along the vertical distance to the substrate. For biofilms on spherical and toroidal surfaces, thickness is measured in the normal direction from the reconstructed interface, as described in the materials

Figure 6. (a) Top (left) and side (right) views of a toroidal droplet containing surface-adherent bacterial biofilm. The scale bars correspond to 500 μm. (b), (c) Projection of all confocal stacks onto the (b) xy and (c) xz planes for toroidal confinement. (d), (e) Projection of all confocal stacks onto the (d) xy and (e) xz planes for spherical confinement. The acceleration of gravity is $\vec{g} = -g\hat{z}$.

section (see figure 2(f) also). A surface normal is defined at every surface element on the interface and each element is identified by its (ρ, ψ) coordinates, at a given z (see figure 3(b)). We then project the surface onto the plane by mapping along the vertical (ρ, ψ) into (x, y) for every z. Since the upper part of the sphere or the torus is not covered by biofilm, this is a one-to-one mapping. The thickness distribution for the sphere, toroid and the planar (silicone solid) interface is shown in figures 7(a), (b) and (c), respectively. The thickness maps indicate a greater thickness toward the bottom of the sphere and the bottom-line of the toroid. To examine this positional variance in detail, we plot the azimuthally averaged thickness and roughness as a function of z. We then indeed see that biofilms on curved surfaces are thickest at the bottom, and progressively thin with height, up to a height z_{max} above which no biofilm is observed (see figures 7(d), (e)). We find that this maximum height is independent of confinement geometry, spherical or toroidal, and defined by a maximum inclination of the interface, $atan \left| \dfrac{\mathrm{d}z}{\mathrm{d}\rho} \right|$ measured along the $\hat{\theta}$ direction, of $(55 \pm 5)^o$. For larger inclinations, the biofilm does not grow. This indicates that gravity plays a role in biofilm growth. For the toroidal case, z_{max} is greater on the inner part of the toroid (see blue curve in figure 7(e)) than on the outer part of the toroid (see green curve in figure 7(e)). This illustrates the more curved and steeper cross-section of the toroid in its outside than in its inside (see figures 6(a), (c)), further confirming the role of gravity in biofilm growth. In contrast, we find that the thickness does not vary with lateral position along the interface for flat substrates, as shown in figure 7(f), further confirming that gravity plays a role in the thickness variation observed for curved interfaces. On the contrary, biofilm roughness is independent of height and position on the interface, as shown in figures 7(g), (h) and (i) for the spherical, toroidal and flat cases, respectively. However, the value of the average biofilm roughness increases by about a factor of two when the substrate is curved (see third column in table 1). Since the observed roughness is not a function of z, this indicates that the change in average roughness is affected by geometry and not by

Figure 7. Comparison of biofilm thickness and roughness distributions on (a), (d), (g) spherical, (b), (e), (h) toroidal, and (c), (f), (i) planar interfaces. The top row panels show the projected thickness distribution on the *xy* plane for (a) spherical, (b) toroidal and (c) planar interfaces. The color scale indicates the *z* position, in microns, of the substrate covered by biofilm. The middle row panels show the azimuthally-average thickness profile as a function of height, *z*, for (d) spherical and (e) toroidal interfaces. For the planar case shown in (f) we average the *x*-dependence for all *y* values. The bottom row panels show the azimuthally-average roughness profile as a function of height, *z*, for (g) spherical and (h) toroidal interfaces. For the planar case shown in (i) we average the *x*-dependence for all *y* values.

gravitational effects. It is likely that curving the interface results in frustrated growth along the normal to the substrate due to crowding, ultimately resulting in a rougher biofilm.

4.2. Oxygen supply and gravitational direction control biofilm growth

Detailed comparison of biofilm location and morphology developed in varying geometries pointed out the importance of oxygen and gravity on regulating biofilm growth. We attributed the biomass accumulation at the top flat surface of the microwell cultures to be oxygen driven. Bacteria tend to thrive at oxygen rich regions where they are most metabolically active. In curved systems where the cell solution is immersed within a single solid phase, biofilms are found at the bottom. Unlike the microwell cultures where all faces except for the top one are oxygen impermeable, the entire substrate of these containers, made of silicone elastomer, is highly permeable to oxygen [27]. The oxygen delivery is thus uniform in all directions. In the absence of different oxygen availability at the top and bottom, there is no driving force for the cells to attach at a higher plane and the biomass accumulates at the bottom of the vessel. The observations in figure 7 suggest that bacterial adhesion to the solid interface is strong enough to maintain the biofilm on an inclined surface. However, the gravitational pull still causes a decrease in biofilm thickness with height. The effect of gravity is further supported by the fact that on curved surfaces, biofilms are no longer observed when the inclination of the interface is greater than a threshold. Consistent with our interpretation that the interplay between oxygen availability and gravity determines where the biofilm grows, experiments conducted with cell solution sandwiched between two silicone solid interfaces, where oxygen availability is equivalent at both interfaces, showed formation of biofilm at the bottom interface. Furthermore, a recent study of *P. aeruginosa* biofilms in microgravity concluded that the effects of gravity on biofilm biomass were minimized when oxygen availability was increased [28], supporting our interpretation that there are competing effects due to gravity and oxygen availability in biofilm growth.

The analysis of the biofilm morphology shows that both the average thickness, maximum thickness, and substratum coverage are the highest for biofilms formed at the air-aqueous interface, followed by those formed at the silicone oil-aqueous interface (see table 1), which indicates that oxygen attracts and helps biofilm growth.

The bio-volume and the biofilm surface-to-volume ratio, $A_{b,e}/V_b$, remain of the same order of magnitude irrespective of the system geometry; this is consistent with having the bacteria reproduce in the presence of identical nutrient supplies, further indicating that they can only grow as fast as the area exposed to the nutrients. This result also suggests that oxygen accessibility is not an issue for the overall cell growth at interfaces surrounded with the silicone matrix. The level of oxygen availability at the interface, however, does have a significant impact on the resulting biofilm morphology. The smallest oxygen supply for silicone oil-aqueous and silicone solid-aqueous interfaces compared to the air-aqueous interface [29], explains the thinner and more sparse biofilm observed in these cases.

To compare the influence of confinement geometry on biofilm growth, we define the relative coverage, Θ_{rel}, as the substratum coverage Θ normalized by the number area density of bacteria N_t/A_t at the start of the experiment, where N_t is the total number of bacteria and A_t is the substrate area. Normalizing Θ in this way accounts for the different area that is accessible to a single bacterium due to the curvature differences between the plane, the sphere and the toroid. Since $\Theta = A_{b,s}/A_t$, then $\Theta_{rel} = A_{b,s}/N_t$, where $A_{b,s}$ is obtained directly from the confocal data and N_t is calculated from the initial cell density and volume of cell solution. We find that Θ_{rel} for curved surfaces is one order of magnitude higher than for flat surfaces (see table 1). This is consistent with the differences in the ratio of the oxygen-exposed-area to confinement volume for the different geometries. For all planar confinements, this ratio is $\mathcal{O}(10^{-4})\,\mu\mathrm{m}^{-1}$, while for spherical and toroidal confinements, this ratio is $\mathcal{O}(10^{-3})\,\mu\mathrm{m}^{-1}$, which is an order of magnitude larger than for the planar cases. Thus, the increase in the surface-to-volume ratio of the confinement geometry promotes the in-plane growth of the biofilm, hence resulting in a larger Θ_{rel}. This difference in relative coverage is accompanied by a difference in biofilm average thickness. Since the biofilm production is similar for all cases, the biofilm growing on flat interfaces must have a larger average thickness than the biofilm growing on curved interfaces, as we indeed see from our thickness measurements; both the average thickness L and an alternative estimate of this quantity from the biovolume and the total biofilm area, V_b/A_b, are larger for the planar interfaces compared to the curved interfaces (see table 1). Thus the biofilm grows laterally to maximize oxygen intake at first, and then vertically once the substrate area is saturated. Curved interfaces possess a larger surface-to-volume ratio, and therefore allow a higher relative coverage of biofilm Θ_{rel} than a flat interface does. Finally, we emphasize that the biofilm roughness R is larger for curved interfaces than for flat interfaces, further emphasizing the role of the confinement geometry over biofilm morphology.

5. Conclusion

We used static culture systems with different solution-interface boundaries to investigate how geometric and other environmental factors affect biofilm formation of *B. subtilis*. We found that *B. subtilis* is capable of forming submerged biofilms, and that the location in which the biofilm develops depends on oxygen accessibility as well as gravity. When the interface is flat and only the top area is oxygen permeable, cells accumulate at the top. When the oxygen is made accessible throughout, biofilms form at the bottom of the vessel. Furthermore, quantitative differences between biofilms on different surfaces are consistent with the change in oxygen availability from one confinement structure to the other. Our results show that geometric factors can be coupled with both oxygen and gravity conditions to influence biofilm growth. In fact, biofilm roughness and relative coverage are both larger for spherical and toroidal confinement geometries than for planar confinement geometries. Provided the nutrient distribution is the same, other gradients than those due to oxygen availability and gravity can play an overriding role, affecting, for example, the morphology of the resultant biofilm.

References

[1] Xavier J B and Foster K R 2007 *Proc. Natl Acad. Sci.* **104** 876–81
[2] Flemming H C and Wingender J 2010 *Nat. Rev. Microbiology* **8** 623–33
[3] Decho A W 2000 *Cont. Shelf Res.* **20** 1257–73
[4] Rogers J, Dowsett A, Dennis P, Lee J and Keevil C 1994 *Appl. Environ. Microbiology* **60** 1842–51
[5] Marsh P 2004 *Caries res.* **38** 204–11
[6] Danhorn T and Fuqua C 2007 *Annu. Rev. Microbiol.* **61** 401–22
[7] Hall-Stoodley L, Costerton J W and Stoodley P 2004 *Nat. Rev. Microbiology* **2** 95–108
[8] Stewart P S and William Costerton J 2001 *Lancet* **358** 135–8
[9] Hochbaum A I and Aizenberg J 2010 *Nano lett.* **10** 3717–21
[10] Chung K K, Schumacher J F, Sampson E M, Burne R A, Antonelli P J and Brennan A B 2007 *Biointerphases* **2** 89–94
[11] Salek M M, Jones S M and Martinuzzi R J 2009 *Biofouling* **25** 711–25
[12] Lee J H, Kaplan J B and Lee W Y 2008 *Biomed. microdevices* **10** 489–98
[13] Drescher K, Shen Y, Bassler B L and Stone H A 2013 *Proc. Natl Acad. Sci.* **110** 4345–50
[14] Stewart P S 2012 *Biofouling* **28** 187–98
[15] Kim M K, Drescher K, Pak O S, Bassler B L and Stone H A 2014 *New J. Phys.* **16** 065024
[16] Branda S S, Gonzalez-Pastor J E, Ben-Yehuda S, Losick R and Kolter R 2001 *Proc. Natl Acad. Sci. USA* **98** 11621–6

[17] Vlamakis H, Chai Y, Beauregard P, Losick R and Kolter R 2013 *Nat. Rev. Microbiology* **11** 157–68

[18] Stewart P S and Franklin M J 2008 *Nat. Rev. Microbiology* **6** 199–210

[19] Zhang W, Seminara A, Suaris M, Brenner M P, Weitz D A and Angelini T E 2014 *New J. Phys.* **16** 015028

[20] Vlamakis H, Aguilar C, Losick R and Kolter R 2008 *Genes Dev.* **22** 945–53

[21] Chai Y R, Chu F, Kolter R and Losick R 2008 *Mol. Microbiology* **67** 254–63

[22] Pairam E and Fernández-Nieves A 2009 *Phys. rev. lett.* **102** 234501

[23] Pairam E, Le H and Fernández-Nieves A 2014 *Phys. Rev.* E **90** 021002

[24] Heydorn A, Nielsen A T, Hentzer M, Sternberg C, Givskov M, Ersbøll B K and Molin S 2000 *Microbiology* **146** 2395–407

[25] Garcia D 2010 *Comput. Stat. Data Anal.* **54** 1167–78

[26] Koza A, Moshynets O, Otten W and Spiers A J 2010 *ISME J.* **5** 665–73

[27] Skolimowski M, Nielsen M W, Emnéus J, Molin S, Taboryski R, Sternberg C, Dufva M and Geschke O 2010 *Lab Chip* **10** 2162–9

[28] Kim W *et al* 2013 *PLoS One* **8** e62437

[29] Charati S and Stern S 1998 *Macromolecules* **31** 5529–35